have exhibited and confirmed quasisteady typical variation. The results displayed by the present hybrid numerical scheme applied to isolated wing and propeller, in quasisteady flow conditions, as well as to coupled configurations, show that the close vortex wing surface interaction gives rise to a low-pressure peak on the wing upper surface, which produces an increase in the positive local lift area near the trailing edge. From a merely computational point of view, the present method has demonstrated its capability to process higher-order mesh refinement and to give accurate results with very low computational effort.

References

[1]Chiaramonte, J. Y., Favier, D., Maresca, C., and Benneceur, S., "Aerodynamic Interaction Study of the Propeller/Wing Different Configurations," *Journal of Aircraft*, Vol. 33, No. 1, 1996, pp. 46–53.

[2]Veldhuis, L. L. M., and Rentema, D. W. E., "Experimental Analysis of the Vortex Wake Structure Behind a Propeller-Wing Configuration," AGARD, CP-584, May 1996.

[3]Witkowski, D., Lee, A., and Sullivan, J., "Aerodynamic Interactions Between Propellers and Wings," *Journal of Aircraft*, Vol. 26, No. 9, 1989, pp. 829–836.

[4]Cho, J., and Williams, M. H., "Propeller-Wing Interaction Using a Frequency Domain Panel Method," *Journal of Aircraft*, Vol. 27, No. 3, 1990, pp. 196–203.

[5]Rottgermann, A., and Wagner, S., "Compressible Potential Flow Around a Helicopter Rotor," *Computational Mechanics*, Vol. 2, Springer–Verlag, New York, 1995, pp. 2915–2920.

[6]Catalano Martini, F., "The Aerodynamic Characteristics of a Smooth Wing at Low Reynolds Number Under Effect of a Pusher Propeller," *Proceedings of the 13th Symposium COBEM-CIDIM'95* (Belo Horizonte, Brazil), available on CD Rom by Microservice, São Paulo, Brazil, 1995.

[7]Kinnas, A. S., and Hsin, C. Y., "Boundary Element Method for the Analysis of the Unsteady Flow Around Extreme Propeller Geometries," *AIAA Journal*, Vol. 30, No. 3, 1992, pp. 688–696.

[8]Graber, A., and Rosen, A., "Velocities Induced by Semi-Infinite Helical Vortex Filaments," *Journal of Aircraft*, Vol. 24, No. 5, 1987, pp. 289, 290.

[9]Yamaguchi, H., and Bose, N., "Oscillating Foils for Marine Propulsion," *Proceedings of the 4th International Offshore and Polar Engineering Conference*, Vol. 3, International Society of Offshore and Polar Engineering, Osaka, Japan, 1994, pp. 539–544.

[10]Bose, N., "Performance of Chordwise Flexible Oscillating Propulsors Using a Time-Domain Panel Method," *International Shipbuilding Progress*, Vol. 432, No. 42, 1995, pp. 281–294.

[11]Müller, R. H. G., Nsi Mba, M., Aymard, E., Favier, D., Berton, E., and Maresca, C., "Visualization and Measurement of Helicopter Rotor Flow with Swept Back Tip Shapes at Hover Flight Using the Flow Visualization Gun Time Line Technique," *Experiments in Fluids*, Vol. 21, No. 3, 1996, pp. 161–169.

[12]Favier, D., and Maresca, C., "Etude du Sillage 3D d'une Hélice Aérienne Quadripale," *AGARD FDP on Aerodynamics and Acoustics of Propellers*, AGARD, CP-366, Oct. 1984. (Paper 15).

[13]Favier, D., Nsi Mba, M., Barbi, C., and Maresca, C., "A Free-Wake Analysis for Hovering Rotors and Advancing Propellers," *Proceedings of the 11th European Rotorcraft Forum* (London), 1985, pp. 493–511 (Paper 21).

[14]Favier, D., Ettaouil, A., and Maresca, C., "Numerical and Experimental Investigation of Isolated Propeller Wakes in Axial Flight," *Journal of Aircraft*, Vol. 26, No. 9, 1989, pp. 837–846.

[15]Ardito Marretta, R. M., and Lombardo, G., "Coefficienti di Trazione, di Coppia e Rendimento dell'Elica in Presenza del Campo Aerodinamico di un'Ala Finita," *Aerotecnica-Missili e Spazio*, Vol. 73, Nos. 1–2, 1994, pp. 31–41.

[16]Ardito Marretta, R. M., "Performance of a Propeller Embedded in the Flowfield of a Wing," *Journal of Aircraft*, Vol. 33, No. 5, 1996, pp. 919–923.

[17]Ardito Marretta, R. M., Davi', G., Lombardi, G., and Milazzo, A., "Wing-Propeller Coupling Simulation from Tractor up to Hover Flight Conditions," *Computer Modeling and Simulation in Engineering*, Vol. 2, No. 3, 1997, pp. 304–321.

[18]Ardito Marretta, R. M., Davi', G., Lombardi, G., and Milazzo, A., "Hybrid Numerical Technique for Evaluating Wing Aerodynamic Loading with Propeller Interference," *Computers and Fluids* (to be published).

[19]Iosilevskii, G., "Lifting-Line Theory of an Arched Wing in Asymmetric Flight," *Journal of Aircraft*, Vol. 33, No. 5, 1996, pp. 1023–1026.

[20]Weissinger, J., "Uber die Auftriebverteilung von Pfeilflugen," *Zentrale fur wissenschaftliches Berichtswesen der Luftfahrtforschung des Generalluftzeug-meisters*," No. 1553, Berlin-Adlershof, 1942.

[21]Prossdorf, S., and Tordella, D., "On an Extension of Prandtl's Lifting Line Theory to Curved Wings," *Impact of Computing in Science and Engineering*, Vol. 3, Nos. 1–3, 1991, pp. 192–212.

[22]Chiocchia, G., and Pignataro, S., "On the Induced Drag Reduction Due to the Propeller-Wing Interaction," *The Aeronautical Journal of the Royal Aeronautical Society*, Vol. 99, No. 988, 1995, pp. 328–336.

[23]Davi', G., Ardito Marretta, R. M., and Milazzo, A., "Explicit Kutta Condition for Unsteady Two-Dimensional High-Order Potential Boundary Element Method," *AIAA Journal*, Vol. 35, No. 6, 1997, pp. 1080, 1081.

[24]Lombardi, G., and Cannizzo, F., "High Aspect Ratio Wings: Tip Vortex Structure and Its Numerical Implications," AIAA Paper 96-1961, July 1996.

Stall Resistance Features of Lifting-Body Airplane Configurations

Joseph Katz* and Shaun Byrne†
San Diego State University, San Diego, California 92182
and
Robert Hahl‡
Redwood Aircraft Corporation, Falls Church, Virginia 22046

Introduction

THE lifting-body airplane concept, pioneered in the early 1920s, seems to fascinate every generation of airplane designers.[1–3] The basic concept, shown in Fig. 1a, postulates that the traditional cylindrical fuselage can be replaced by an airfoil-shaped body that contributes to the airplane lift. The design allows for larger cabin volume and, possibly, less wing loading during takeoff and landing because of the additional lift of the body. The generic model of Fig. 1a depicts the features of the early designs, which had small aspect-ratio airfoil-shaped fuselages (when viewed from the side) and a quite angular rectangular shape (when viewed from the top). The sharp side edges of those early designs created sizable vortex lift at the higher angles of attack, and the resulting large drag increase may have hurt the appeal of the concept.

Another approach to airplane design is based on eliminating the fuselage entirely, leading to the flying wing concept. This approach allows a spanwise continuous wing without interruptions by fuselage junctions. However, for small airplanes, the small wing thickness severely limits cabin heights. Therefore, for such a design to be practical, only large airplanes can be considered. Recent studies of such large transport aircraft[4] propose the blended wing concept, which, in essence, is a com-

Presented as Paper 98-0760 at the AIAA 36th Aerospace Sciences Meeting, Reno, NV, Jan. 12–15, 1998; received Feb. 4, 1998; revision received Aug. 25, 1998; accepted for publication Aug. 28, 1998.

*Professor, Department of Aerospace Engineering and Engineering Mechanics. Associate Fellow AIAA.

†Student, Department of Aerospace Engineering and Engineering Mechanics. Member AIAA.

‡President and CEO.

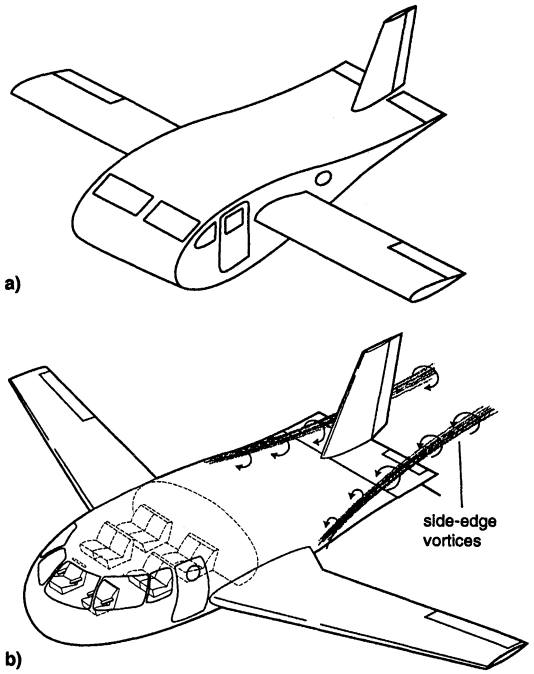

Fig. 1 a) Original lifting-body concept with a two-dimensional airfoil shape, and b) the modified shape suitable for small business-jet applications. Note the sketch of side-edge vortices visible above the aft section of the fuselage at angles of attack larger than 6 deg.

bination of the Burnelli lifting body and the flying wing concepts. The present study focuses on applying some of the preceding principles to a small entry-level business-jet airplane configuration (6–10 passengers), where the more spacious fuselage results in additional advantages over the traditional cylindrical fuselage shape. A desirable cabin height of 1.85 m (compared with 1.45–1.60 m of current entry-level jets), combined with four abreast seating, results in a fairly large body (as shown in Fig. 1b). By rounding the edges of the fuselage (from the front view), the lift/drag ratio (L/D) of the configuration can be improved to a level on par with other contemporary designs. The large internal volume, compared with conventional airplanes of the same class, not only allows a wider and taller cabin, but also provides room for additional internal fuel storage (for extended range), and allows much thinner wings for transonic cruise. The fuselage orientation in this concept of Fig. 1b is dictated by minimum drag at cruise; therefore, it is aligned with the direction of flight (at cruise). However, during takeoff and landing, the fuselage can contribute to the airplane lift, thereby reducing the required size and complexity of the wing-mounted high-lift devices (hence, cost and weight savings, see Ref. 5). For simplicity, the fuselage of the generic lifting-body configuration tested here is based on elliptic sections, and small-scale wind-tunnel tests were used to evaluate its aerodynamic performance. The main objectives of the study were the investigation of the low-drag potential at cruise condition and the high-lift and poststall characteristics, e.g., stall resistance, of such configurations during takeoff and landing.

Model and Test Procedure

The basic dimensions of the generic 1:20 scale business-jet model are shown in Fig. 2. From the side view, the lifting body is defined by an 18% thick NACA 63_3-018 airfoil section with its maximum thickness located at 35% of the length, measured from the nose. At this maximum thickness location, the body had an aspect ratio 2.2 elliptic cross section (from the front view). The nose shape, from the top view, followed the contours of a semiellipse (up to the 35% point), and from this

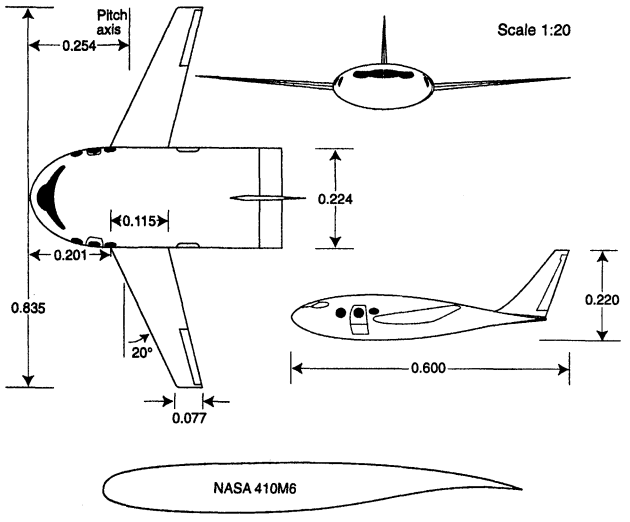

Fig. 2 Basic dimensions of the wind-tunnel model.

point to the tail the fuselage aft section had a constant width, as shown in Figs. 1b and 2. These two views (top and side) define the major and minor axes of the elliptical cross sections at each longitudinal station, ending with a horizontal line at the trailing edge. A 12%-thick transonic airfoil section (NASA 410M6) was used for the untwisted wing, and its shape is shown at the bottom of Fig. 2.

Airspeed at the wind tunnel was set at 45 m/s, resulting in a wing-chord-based Reynolds number of about 0.4×10^6. Freestream turbulence levels were less than 0.5%, and no boundary-layer tripping devices were used on the model wing or fuselage (and so free transition is assumed). Test section dimensions are 0.91 m height by 1.22 m width, with frontal blockage beginning below 2%, and increasing slightly above 4% at angles of attack over 20 deg. Therefore, no blockage corrections were applied to the data presented here. Estimated uncertainty of the data, including the accuracy of the six-component scale, airspeed measurements errors, and data reduction system uncertainties, is less than $C_L = \pm 0.01$, $C_D = \pm 0.005$, and $C_M = \pm 0.01$. A reference area of $A_R = 831$ cm^2 and a reference chord of $c_R = 11.2$ cm was used for the data reduction.

Results

The near-cylindrical fuselage used for most conventional aircraft develops very little lift (compared with the contribution of the wings) during landing and takeoff. Using the fuselage to create sizable lift can reduce the size and complexity of wing-mounted high-lift systems, but early configurations (as in Fig. 1a) suffered from relatively high drag. Figure 3 shows the basic lift and drag variation vs angle of attack for the present configuration, and clearly, the drag is comparable with conventional airplane data.[6] Another interesting aerodynamic feature visible in Fig. 3 is the shape of the lift curve, where the lift coefficient increases with angle of attack, even beyond the point of wing stall, as shown by the arrow.

Because of the low Reynolds number of this test and the 12% thin transonic airfoil section (NASA 410M6), the wing stall begins quite early at about 5-deg angle of attack (α). However, as noted, in spite of the early wing stall, the configuration lift coefficient increases up and beyond $\alpha = 20$ deg because of the vortex lift of the fuselage. Because of the mechanical limits of the experiment, angles of attack larger than $\alpha = 20$ deg could not be obtained, and the lift-stall of the total configuration was not reached. Flow visualization with this model indicated that as the angle of attack increases beyond about $\alpha = 6$ deg, two side-edge vortices are formed above the fuselage aft section (see Fig. 1b). This vortex flow is visible at $\alpha = 6$ deg and seems to increase in strength above $\alpha = 11$

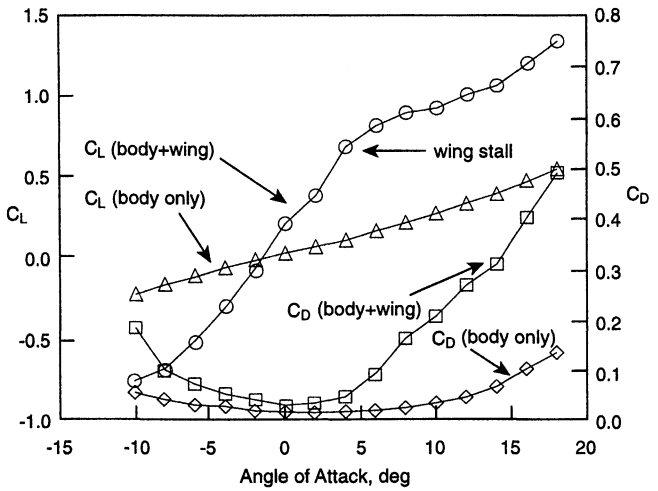

Fig. 3 ***L/D*** **variation vs angle of attack for the basic lifting-body configuration and for the fuselage alone (*Re* = 0.4 × 10^6, scale 1:20).**

deg. The expected effect of these aft-positioned vortices is the increase of the lift at the higher angles of attack, contributing to a nose-down pitching moment (which may be considered a stall-resistant feature). Also, at these larger angles of attack, the lift carryover across the wide fuselage (seen by computations not reported here) reduces the effect of the opposite-rotation wing-root vortices, on the dominant side-edge vortices shown in Fig. 1b. Furthermore, rolling moment data (not presented here) stayed close to zero throughout the angle-of-attack sweep presented here, indicating no side vortex asymmetry.

Angle of attack in the present experiment was measured relative to the body's centerline, and at $\alpha = 0$ the lift coefficient is about $C_L = 0.22$ (see Fig. 3), yielding a zero lift angle of about -1.5 deg for the configuration. Zero lift drag at this condition is estimated to be slightly less than $C_D \approx 0.025$, a value that was expected to improve at a higher Reynolds number, making this configuration quite competitive within the business-jet category. (During the experiments, a limited trailing-edge separation was visible on this transonic wing section, which is expected to disappear at full-scale Reynolds number conditions. On the other hand, fuselage drag may increase because of an earlier transition, but the combined effect is expected to improve *L/D*.) This relatively low drag is particularly important in view of the large drag created by the early lifting body concepts that had sharp edges around their two-dimensional airfoil-shaped fuselages. Beyond the angle of wing stall ($\alpha = 6$ deg), wing drag increases sharply, dictating the large increase in the total drag as shown in Fig. 3. This effect is a result of the low Reynolds number of the small-scale testing, but both wing stall and drag increase are expected to be delayed at larger scales.

To investigate the large drag increase beyond wing stall, the lifting-body fuselage was tested separately (without the wings), in an effort to isolate the aerodynamic characteristics of the fuselage from the data of the complete configuration. Results of this test are presented in Fig. 3. The circular and rectangular symbols represent the data for the complete configuration, whereas the triangular and diamond symbols stand for the fuselage alone. Clearly, the fuselage lift increases quite monotonically and the drag polar is quite shallow, emphasizing that the large drag increase is a result of the wing stall only. *L/D* of the body (not shown) increases up to about 8.2 at an angle of attack of $\alpha = 10$ deg, and a lift stall was not detected within the angle-of-attack range of the experiment. The ability of the fuselage to create a lift coefficient of about 0.5 is quite significant, and for unmanned airplane applications, where the vehicle can be pitched up beyond $\alpha = 20$ deg, this may be utilized as an effective high-lift device.

The *L/D* for the complete model (with wings) is presented in Fig. 4, and a value close to 16 was obtained before the wing stalled, at about $\alpha = 4$ deg. The abrupt drop in *L/D* is a direct result of the wing stall, and as mentioned, at higher Reynolds numbers, e.g., at full scale, the ratio is expected to rise as a result of the delay of the wing stall. Algebraic manipulation of the uncertainty of lift and drag shows an uncertainty of ± 1.8 in the *L/D* data; however, repeated experiments showed that the uncerainty in *L/D* is closer to ± 0.3. The pitching moment curve in Fig. 4 indicates that beyond the wing stall, the c.p. moves backward, creating a nose-down moment. At angles of attack beyond $\alpha = 11$ deg, the side-edge vortices increase in strength, and the resulting nose-down moment increases. This effect is visible by the change in the negative slope of C_M in Fig. 4, and may be considered as a stall-resistant feature with important safety-related implications. Note that C_M is measured relative to the scale centerline (see Fig. 2), which is obviously ahead of the c.p. (hence, the negative slope). This pitching axis results in a static margin (for -5 deg $< \alpha < 5$ deg) of about 0.113, suggesting that for additional longitudinal stability, the actual c.g. could be moved forward of this point.

The side-edge vortices (shown in Fig. 1b), responsible for the stall-resistant nature of the lifting body, are affected by parameters such as side-edge curvature and aft-body taper. One of these effects, the fuselage taper, was investigated briefly by changing the fuselage side-edge angle (behind the point of the body's maximum thickness at 35%) by ± 10 deg, as shown in the inset to Fig. 5. The measured pitching moment coefficients for the three aft-body tapers are also presented in Fig. 5, and additional data on the model lift and drag are presented in Ref. 7. In general, the effect of the aft-body becomes more pronounced at angles of attack beyond stall, where most of the lift is created by the fuselage. The drag follows similar trends, particularly at higher angles of attack, and it increases slightly with increased aft-fuselage width.[7] Also, the wide tail configuration produces more lift than the straight and the narrow tail configuration, correspondingly. The effect of aft-body taper on the *L/D* is quite small, and the configuration with the narrow tail reached a peak of over 16, whereas the ratio for the wide tail was about 15.5 (compared with 16 for the untapered body).

The effect of the aft-body taper is more pronounced in the pitching-moment diagram of Fig. 5. This is a direct result of the vortex lift shown in Fig. 1b, which in the case of the wide tail becomes quite large as angle of attack increases. Clearly, the wide tail shape has the most nose-down moment, particularly beyond wing stall, making it the most stall-resistant shape out of the three shown. Incorporating such data into the preliminary design of an airplane configuration allows the tai-

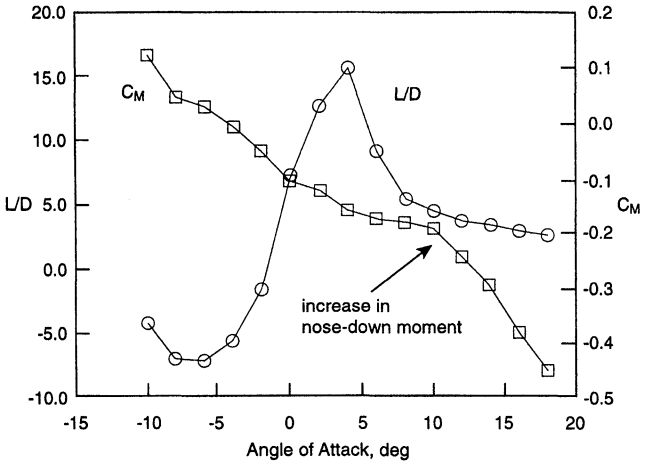

Fig. 4 ***L/D*** **and pitching moment variation vs angle of attack (*Re* = 0.4 × 10^6, scale 1:20).**

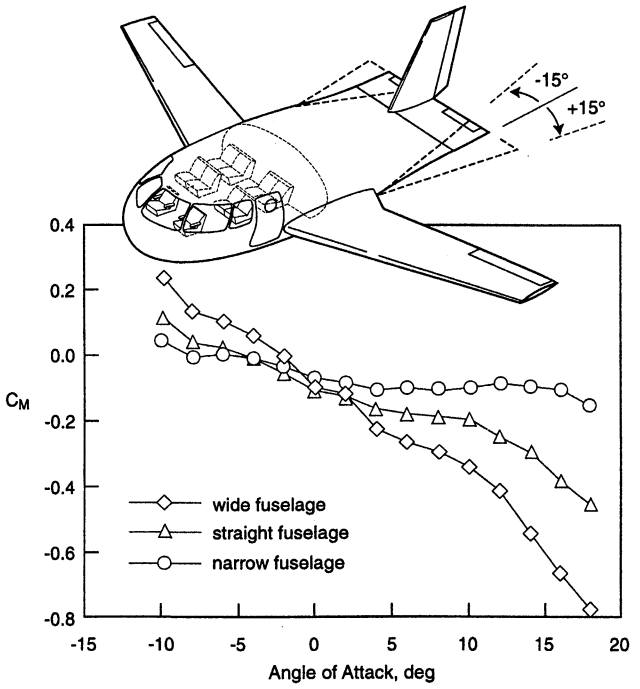

Fig. 5 Effect of aft-fuselage taper on pitching moment (Re = 0.4 × 10^6, scale 1:20).

loring of the sudden increase in the pitching-moment slope into a desirable angles-of-attack range. Therefore, when an airplane's c.g. calculations and elevator sizing are complete, the use of these data can make airplane stall unreachable.

Concluding Remarks

The experimental data presented here indicate that a small aircraft with a wide lifting-body fuselage can benefit, in addition to the large cabin size, from several unique aerodynamic features. The configuration can reach quite high lift coefficients because of the fuselage vortex lift, without sacrificing the L/D at low angles of attack. The high-angle-of-attack vortex lift at the aft section of the fuselage causes a large nose-down pitching moment, which can be utilized for a stall-safe design. Finally, the basic principle of using the fuselage as a simple and cheap high-lift device was demonstrated.

Acknowledgment

The authors wish to thank Stig Johansson for his help in designing, building, and testing the wind-tunnel model.

References

[1]Cantilli, E. J., "Saga of the Lifting Body/Flying Wing," *Flight Journal*, Vol. 1, No. 2, 1996, pp. 56–61.

[2]*Jane's Encyclopedia of Aviation*, Vol. 2, Jane's Information Group, Ltd., Coulsdon, Surrey, UK, 1980, p. 367.

[3]Mitchell, K. A., "Burnelli and His Lifting-Body Transports," *American Aviation Historical Society Journal*, Spring 1997, pp. 2–19.

[4]Liebeck, R. H., Page, M. A., and Rawdon, B. K., "Blended-Wing-Body Subsonic Commercial Transport," AIAA Paper 98-0438, Jan. 1998.

[5]Hahl, R., and Katz, J., "Lifting-Fuselage/Wing Aircraft Having an Elliptical Forebody," U.S. Patent Appl. 08-642997, May 13, 1996.

[6]Raymer, D. P., *Aircraft Design: A Conceptual Approach*, AIAA Educational Series, AIAA, Washington, DC, 1992, Chap. 12.

[7]Katz, J., Byrne, S., and Hahl, R., "Stall Resistance Features of Lifting-Body Airplane Configurations," AIAA Paper 98-0760, Jan. 1998.

Application of Active Separation Control to a Small Unmanned Air Vehicle

A. Seifert,* T. Bachar,† and I. Wygnanski‡
Tel-Aviv University, Tel-Aviv 69978, Israel
and
A. Kariv,§ H. Cohen,¶ and R. Yoeli**
Aero Design and Development, Inc., Rehovot 76102, Israel

Introduction

THE delay of boundary-layer separation by oscillatory injection of momentum established the superiority of the method over steady blowing.[1] The performance of various airfoils was improved, even when separation was not entirely avoided. Although the addition of small amounts of steady blowing to the fluctuating momentum slightly reduces the efficiency of the excitation, the application of steady blowing may require two orders of magnitude greater momentum coefficient for similar gains in performance. While most wind-tunnel experiments used external devices to excite the flow, a self-contained system is required for active flow control in flight. Furthermore, mounting an active flow control device on an unmanned air vehicle (UAV) or an airplane model allows one to test its effectiveness as an alternate control surface. This Note describes wind-tunnel experiments on a UAV to which active separation control was added to improve its performance and to exercise roll authority in an unconventional manner.

Approach

The project was subdivided into four intermediate stages:

1) The application of oscillatory and steady blowing to a flapped Eppler 214 airfoil. The oscillatory blowing was initially provided by an external mechanism.[2] Some of the results were presented in Ref. 1 and they will not be discussed here.

2) The development of a self-contained oscillatory blowing system.

3) The installation of the system on the UAV and full-scale tests in a low-speed, industrial wind tunnel.

4) Actual flight tests of the UAV with active separation control.

The quantitative results obtained during stage 3 are reported in this Note.

Experiment

A scaled down Scout UAV was used in the experiment, but its original wing was replaced with a wing based on the Eppler 214 airfoil of a larger span. A simply hinged, 30% chord, trailing-edge flap and ailerons spanned the outer section of the

Received July 8, 1998; revision received Aug. 31, 1998; accepted for publication Sept. 15, 1998.

*Engineer, Fluid Mechanics and Heat Transfer Department; currently on leave from Tel-Aviv University, National Research Council Researcher, NASA Langley Research Center, M/S 170, Hampton, VA 23681. Member AIAA.

†Engineer, Department of Fluid Mechanics and Heat Transfer.

‡Professor, Fluid Mechanics and Heat Transfer Department; also AME Department, University of Arizona, Tucson, AZ 85721. Fellow AIAA.

§Aerodynamic Project Manager.

¶Team Leader, System Engineering.

**Managing Director.